

1 Universal behavior of dispersive Dirac cone in gradient index plasmonic metamaterials

2 Matthias Maier,^{1,*} Marios Mattheakis,^{2,†} Efthimios Kaxiras,^{2,3} Mitchell Luskin,¹ and Dionisios Margetis⁴

3 ¹*School of Mathematics, University of Minnesota, Minneapolis, Minnesota 55455, USA*

4 ²*School of Engineering and Applied Sciences, Harvard University, Cambridge, Massachusetts 02138, USA*

5 ³*Department of Physics, Harvard University, Cambridge, Massachusetts 02138, USA*

6 ⁴*Department of Mathematics, and Institute for Physical Science and Technology,*
7 *and Center for Scientific Computation and Mathematical Modeling,*
8 *University of Maryland, College Park, Maryland 20742, USA.*

9 (Dated: Draft of January 9, 2018)

We demonstrate analytically and numerically that the dispersive Dirac cone emulating an epsilon-near-zero (ENZ) behavior is a universal property within a family of plasmonic crystals consisting of two-dimensional (2D) metals. Our starting point is a periodic array of 2D metallic sheets embedded in an *inhomogeneous and anisotropic* dielectric host that allows for propagation of transverse-magnetic (TM) polarized waves. By invoking a systematic bifurcation argument for arbitrary dielectric profiles in one spatial dimension, we show how TM Bloch waves experience an effective dielectric function that averages out microscopic details of the host medium. The corresponding effective dispersion relation reduces to a Dirac cone when the conductivity of the metallic sheet and the period of the array satisfy a critical condition for ENZ behavior. Our analytical findings are in excellent agreement with numerical simulations.

10 I. INTRODUCTION

11 In the past few years the dream of manipulating the
12 laws of optics at will has evolved into a reality with the
13 use of metamaterials. These structures have made it
14 possible to observe aberrant behavior like no refraction,
15 referred to as epsilon-near-zero (ENZ)^{1–5}, and negative
16 refraction⁶. This level of control of the path and dis-
17 persion of light is of fundamental interest and can lead
18 to exciting applications. In particular, plasmonic meta-
19 materials offer significant flexibility in tuning permittivity
20 or permeability values. This advance has opened
21 the door to novel devices and applications that include
22 optical holography⁷, tunable metamaterials^{8,9}, optical
23 cloaking^{10,11}, and subwavelength focusing lenses^{12,13}.

24 Plasmonic crystals, a class of particularly interesting
25 metamaterials, consist of stacked metallic layers arranged
26 periodically with subwavelength distance, and embed-
27 ded in a dielectric host. These metamaterials offer new
28 ‘knobs’ for controlling optical properties and can serve
29 as negative-refraction or ENZ media^{14–16}. The advent
30 of truly two-dimensional (2D) materials with a wide
31 range of electronic and optical properties, comprising
32 metals, semi-metals, semiconductors, and dielectrics¹⁷,
33 promise exceptional quantum efficiency for light-matter
34 interaction¹⁸. In this paper, we characterize the ENZ
35 behavior of a wide class of plasmonic crystals by using a
36 general theory based on Bloch waves.

37 The ultra-subwavelength propagating waves (plas-
38 mons) found in plasmonic crystals based on 2D met-
39 als, in addition to providing extreme control over optical
40 properties^{19–22}, also demonstrate low optical losses due
41 to reduced dimensionality^{5,6}. In particular, graphene is
42 a rather special 2D plasmonic material exhibiting ultra-
43 subwavelength plasmons, and a high density of free car-
44 riers which is controllable by chemical doping or bias
45 voltage^{21,23–25}. An important finding is that the ENZ

46 behavior introduced by subwavelength plasmons is char-
47 acterized by the presence of dispersive Dirac cones in
48 wavenumber space^{2–5}. This linear iso-frequency disper-
49 sion relation was shown for the special case of plas-
50 monic crystals containing 2D dielectrics with spatial-
51 independent dielectric permittivity. This relation re-
52 quires precise tuning of system features⁵. It is not clear
53 from this earlier result to what extent the ENZ behav-
54 ior depends on the homogeneity of the 2D dielectric, or
55 could be generalized to a wider class of materials.

56 In this paper, we show that the occurrence of disper-
57 sive Dirac cones in wavenumber space is a *universal* prop-
58 erty in plasmonic crystals with dielectrics characterized
59 by *any spatial-dependent dielectric permittivity* within a
60 class of anisotropic materials. We provide an exact ex-
61 pression for the critical structural period at which the
62 multilayer system behaves as an ENZ medium. This dis-
63 tance between adjacent sheets depends on the permittiv-
64 ity profile of the dielectric host as well as on the surface
65 conductivity of the 2D metallic sheets. In addition, we
66 give an analytical derivation and provide computational
67 evidence for our predictions. To demonstrate the applica-
68 bility of our approach, we investigate numerically electro-
69 magnetic wave propagation in *finite* multilayer plasmonic
70 structures, and verify the ENZ behavior at the predicted
71 structural period. These results suggest a systematic ap-
72 proach to making general and accurate predictions about
73 the optical response of metamaterials based on 2D mul-
74 tilayered systems. An implication of our method is the
75 emergence of an *effective* dielectric function in the dis-
76 persion relation, which can be interpreted as the result
77 of an averaging procedure (homogenization). This view
78 further supports the universal character of our theory.

79 The remainder of the paper is organized as follows. In
80 Sec. II, we introduce the problem geometry and general
81 formulation by Bloch-wave theory. Section III outlines
82 the exactly solvable example of parabolic permittivity of



FIG. 1: Geometry of the plasmonic crystal. The layered structure is periodic in the x -direction and consists of planar 2D metallic sheets with isotropic conductivity σ .

the dielectric host. In Sec. IV, we develop a bifurcation argument that indicates the universality of the dispersion relation and ENZ behavior for a class of plasmonic crystals. Section V concludes our analysis by pointing out a linkage of our results to the homogenization of Maxwell's equations. The $e^{-i\omega t}$ time dependence is assumed throughout, where ω is the angular frequency. We write $f = \mathcal{O}(h)$ to imply that $|f/h|$ is bounded in a prescribed limit.

II. GEOMETRY AND BLOCH-WAVE THEORY

In this section, we describe the geometry of the problem and the related Bloch-wave theory. Consider a plasmonic crystal that is periodic in the x -direction and consists of flat 2D metallic sheets with isotropic surface conductivity σ (see Fig. 1). Each sheet is parallel to the yz -plane and positioned at $x = nd$ for integer n .

The material filling the space between any two consecutive sheets is described by the anisotropic relative permittivity tensor $\text{diag}(\varepsilon_x, \varepsilon_y, \varepsilon_z)$, where $\varepsilon_x = \text{constant}$, and $\varepsilon_y(x) = \varepsilon_z(x)$ depends on the spatial coordinate x with period d . Here, we set the vacuum permittivity equal to unity, $\varepsilon_0 = 1$. We seek solutions of time-harmonic Maxwell's equations with transverse-magnetic (TM) polarization, that is, with electric and magnetic field components $\mathbf{E} = (E_x, 0, E_z)$ and $\mathbf{H} = (0, H_y, 0)$. The assumed TM-polarization and the symmetry of the physical system suggest that

$$E_z(x, z) = \mathcal{E}(x) e^{ik_z z},$$

which effectively reduces the system of governing equations to a 2D problem. Substituting the above ansatz into time-harmonic Maxwell's equations and eliminating E_x and H_y leads to the following ordinary differential equation for $\mathcal{E}(x)$:

$$-\partial_x^2 \mathcal{E} + \kappa(k_z) \varepsilon_z(x) \mathcal{E} = 0, \quad \kappa(k_z) = \frac{k_z^2 - k_0^2 \varepsilon_x}{\varepsilon_x}, \quad (1)$$

where μ denotes the permeability of the ambient material and $k_0 = \omega\sqrt{\mu}$. By the continuity of the tangential electric field and the jump discontinuity of the tangential magnetic field due to surface current, the metallic sheets give rise to the following transmission conditions

at $x = nd$:

$$\begin{cases} \mathcal{E}^+ = \mathcal{E}^-, \\ -i(\omega/\sigma) \left[(\partial_x \mathcal{E})^+ - (\partial_x \mathcal{E})^- \right] = \kappa(k_z) \mathcal{E}^+, \end{cases}$$

where $(\cdot)^\pm$ indicates the limit from the right (+) or the left (-) of the metallic boundary. In order to close the system of equations, we make a Bloch-wave ansatz in the x -direction, with k_x denoting the real Bloch wavenumber:

$$\mathcal{E}(x) = e^{ik_x d} \mathcal{E}(x - d), \quad \partial_x \mathcal{E}(x) = e^{ik_x d} \partial_x \mathcal{E}(x - d).$$

The combination of the transmission conditions and the periodicity assumption leads to a closed system consisting of Eq. (1) and the following boundary conditions:

$$\begin{bmatrix} \mathcal{E}(d^-) \\ \mathcal{E}'(d^-) \end{bmatrix} = e^{ik_x d} \begin{bmatrix} 1 & 0 \\ -i(\sigma/\omega)\kappa(k_z) & 1 \end{bmatrix} \begin{bmatrix} \mathcal{E}(0^+) \\ \mathcal{E}'(0^+) \end{bmatrix},$$

with $\mathcal{E}'(x) = \partial_x \mathcal{E}(x)$.

We next describe the *dispersion relation* between k_x and k_z in general terms. In the following analysis, we work in the 2D wavenumber space with $\mathbf{k} = (k_x, k_z)$. To render Eqs. (1) with the above boundary conditions amenable to analytical and numerical investigation, we perform an additional algebraic manipulation: Let $\mathcal{E}_{(1)}(x)$ and $\mathcal{E}_{(2)}(x)$ be solutions of Eq. (1) with initial conditions

$$\mathcal{E}_{(1)}(0) = 1, \quad \mathcal{E}'_{(1)}(0) = 0, \quad \mathcal{E}_{(2)}(0) = 0, \quad \mathcal{E}'_{(2)}(0) = 1. \quad (2)$$

These solutions are linearly independent and therefore the general solution for $\mathcal{E}(x)$ is given by $\mathcal{E}(x) = c_1 \mathcal{E}_{(1)}(x) + c_2 \mathcal{E}_{(2)}(x)$. The existence of a non-trivial solution implies the condition

$$D[\mathbf{k}] = \det \left(e^{ik_x d} \begin{bmatrix} 1 & 0 \\ -i(\sigma/\omega)\kappa(k_z) & 1 \end{bmatrix} - \begin{bmatrix} \mathcal{E}_{(1)}(d) & \mathcal{E}_{(2)}(d) \\ \mathcal{E}'_{(1)}(d) & \mathcal{E}'_{(2)}(d) \end{bmatrix} \right) = 0. \quad (3)$$

Equation (3) expresses an implicit dispersion relation, namely, the locus of points \mathbf{k} such that $D[\mathbf{k}] = 0$.

III. AN EXAMPLE: PARABOLIC DIELECTRIC PROFILE

For certain permittivity profiles $\varepsilon_z(x)$ of period d , the system of Eqs. (1) and (2) admits exact, closed-form solutions. Thus, Eq. (3) is made explicit. Next, we present analytical and computational results for a parabolic permittivity profile $\varepsilon_z(x)$. Note that the case of constant permittivity, $\varepsilon_z(x) = \text{const.}$, is analyzed in Ref. 5.

Accordingly, consider the *parabolic* dielectric profile

$$\varepsilon_z(x) = \varepsilon_{z,0} \left[1 + 6\alpha \frac{x}{d} \left(1 - \frac{x}{d} \right) \right], \quad (4)$$

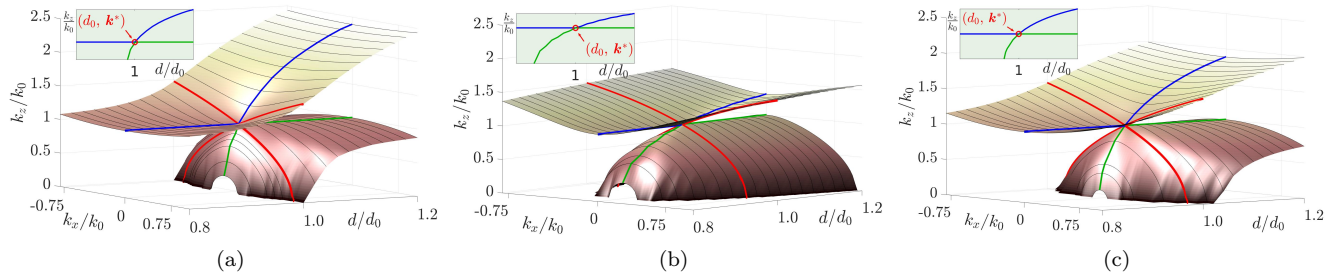


FIG. 2: Parameter study of numerically computed dispersion curves for (a) the parabolic profile (4) with the scaling parameter $\alpha = 20/3$, (b) double-well profile f_{dw} and (c) non-symmetric profile f_{ns} . d/d_0 is chosen in the range from 0.8 to 1.2. The red solid lines indicate the Dirac cones dispersion at $d = d_0$. The inset shows the dispersion relation at the center of the Brillouin zone \mathbf{k}^* as function of d (blue and green cutlines in the major image).

152 which is well known in optics^{26,27}. Here, $\alpha > 0$ is a
 153 scaling parameter with background dielectric permittivity
 154 $\varepsilon_{z,0} > 0$. In this case, $\mathcal{E}_{(1)}$ and $\mathcal{E}_{(2)}$ can be written in
 155 terms of closed-form special functions (see Appendix A).
 156 Relation (3) can be further simplified in the vicinity of
 157 the center of the Brillouin zone, where $|k_x d| \ll 1$, by
 158 choosing the branch of the dispersion relation containing
 159 $\mathbf{k}^* = (k_x^*, k_z^*) = (0, \pm k_0 \sqrt{\varepsilon_x})$. As a result of this sim-
 160 plification, the Bloch wave sees a homogeneous medium
 161 with effective permittivity $\varepsilon = \text{diag}(\varepsilon_x, \varepsilon_z^{\text{eff}}, \varepsilon_z^{\text{eff}})$. The
 162 dispersion relation is

$$\frac{k_x^2}{\varepsilon_z^{\text{eff}}} + \frac{k_z^2}{\varepsilon_x} = k_0^2, \quad \frac{\varepsilon_z^{\text{eff}}}{\varepsilon_{z,0}} = 1 + \alpha - \frac{\xi_0}{d}. \quad (5)$$

163 In the above, ξ_0 denotes the plasmonic thickness, $\xi_0 =$
 164 $-i\sigma/(\omega\varepsilon_{z,0})$ ^{5,6,20}. Here, we assume for the sake of argu-
 165 ment that σ is a purely imaginary number so that ξ_0 is
 166 real valued. Below, we will provide a derivation of (5) for
 167 general profiles $\varepsilon_z(x)$. Dispersion relation (5) is valid in a
 168 neighborhood of \mathbf{k}^* . For $\varepsilon_z^{\text{eff}} \geq 0$, this relation describes
 169 an elliptic, or hyperbolic band, respectively.

170 The ENZ behavior is characterized by $\varepsilon_z^{\text{eff}} \approx 0$ in dis-
 171 persion relation (5)⁵. In the case of the parabolic profile
 172 of this section, this condition is achieved if $\xi_0/d = 1 + \alpha$.
 173 This motivates the definition of the critical ENZ struc-
 174 tural period,

$$d_0 = \xi_0 / (1 + \alpha). \quad (6)$$

175 A breakdown of Eq. (5) due to $\varepsilon_z^{\text{eff}} = 0$ is a necessary
 176 condition to observe linear dispersion and thus disper-
 177 sive Dirac cones⁵. Even though Eq. (5) is an approximate
 178 formula describing the dispersion relation in the neigh-
 179 borhood of \mathbf{k}^* , the ENZ condition $d = d_0$ is exact for the
 180 existence of a Dirac cone for this example of a parabolic
 181 profile.

182 In the case with a lossy metallic sheet, when σ has pos-
 183 itive real part, d_0 becomes a complex-valued number and,
 184 thus, the ENZ condition $d = d_0$ cannot be satisfied ex-
 185 actly. However, for all practical purposes, losses are typ-

186 ically very small such that an effective ENZ behavior can
 187 be approximately observed with the choice $d = \text{Re}(d_0)$.

188 We now verify the effective theory given by Eqs. (5)
 189 and (6) numerically. In order to compute all real-valued
 190 dispersion bands located near \mathbf{k}^* , we solve the system of
 191 Eqs. (1), (2), and (3) (for details see Appendix B). We
 192 carry out a parameter study with the scaling parameter
 193 $\alpha = 20/3$, background permittivity components $\varepsilon_{z,0} = 2$
 194 (in-plane) and $\varepsilon_x = 1$ (out-of-plane), and d/d_0 in the
 195 range from 0.8 to 1.2. The numerically computed disper-
 196 sion bands are shown in Fig. 2a. A band gap appears for
 197 values of d different than d_0 .

198 IV. UNIVERSALITY OF DISPERSION 199 RELATION AND ENZ CONDITION

200 In this section, we address the problem of arbitrary
 201 $\varepsilon_z(x)$, both analytically and numerically. We claim that
 202 effective dispersion relation (5) and ENZ condition (6)
 203 are in fact *universal* within the model of Sec. II. This
 204 means that they are valid for any tensor permittivity
 205 $\text{diag}(\varepsilon_x, \varepsilon_z, \varepsilon_z)$ with arbitrary, spatial-dependent $\varepsilon_z(x)$.
 206 To develop a general argument, we set

$$\varepsilon_z(x) = \varepsilon_{z,0} f(x/d), \quad f(x) > 0, \quad (7)$$

207 where $f(x)$ is an arbitrarily chosen, continuous and pe-
 208 riodic positive function. Guided by our results for the
 209 parabolic profile (Sec. III), we now make the conjecture
 210 that dispersion relation (5) still holds with the definitions

$$d_0 = \xi_0 \left[\int_0^1 f(x) dx \right]^{-1}, \quad \frac{\varepsilon_z^{\text{eff}}}{\varepsilon_{z,0}} = \xi_0 \left(\frac{1}{d_0} - \frac{1}{d} \right). \quad (8)$$

211 In the following analysis, we give a formal bifurcation
 212 argument justifying definition (8). We start by expand-
 213 ing Eq. (3) in the neighborhood of \mathbf{k}^* in powers of the
 214 components of $\delta\mathbf{k} = (\delta k_x, \delta k_z) = \mathbf{k}^* - \mathbf{k}$. First, it can
 215 be readily shown that at $\mathbf{k} = \mathbf{k}^*$ Eq. (1) reduces to
 216 $-\partial_x^2 \mathcal{E} = 0$. Thus, the system of fundamental solutions

is given by $\mathcal{E}_{(1)}(x) = 1$, $\mathcal{E}_{(2)}(x) = x$. This implies that $D[\mathbf{k}^*] = 0$. The expansion of $D[\mathbf{k}]$ up to second order in $\delta\mathbf{k}$ leads to an expression of the form

$$D[\mathbf{k}^* + \delta\mathbf{k}] = b_x \delta k_x + b_z \delta k_z + b_{xx} (\delta k_x)^2 + b_{zz} (\delta k_z)^2 + b_{xz} \delta k_x \delta k_z.$$

The occurrence of a Dirac point is identified with the appearance of a critical point for $D[\mathbf{k}]$, when $b_x = b_z = 0$. In order to express b_x and b_z in terms of physical parameters, we notice that only the term $[ie^{ik_x d}(\sigma/\omega)\kappa(k_z) + \mathcal{E}'_{(1)}(d)] \mathcal{E}_{(2)}(d)$ of $D[(k_x, k_z)]$ contributes to first order in $\delta\mathbf{k}$. Accordingly, we find

$$D[\mathbf{k}^* + \delta\mathbf{k}] = -d \left(\frac{-i\sigma}{\omega \varepsilon_x} 2k_z \delta k_z - \delta \mathcal{E}'_{(1)}(d) [\delta k_z] \right) + \mathcal{O}((\delta\mathbf{k})^2).$$

Here, $\delta\mathcal{E}[\delta k_z]$ denotes the total variation of \mathcal{E} with respect to k_z in the direction δk_z . It can be shown (see Appendix B) that $\delta\mathcal{E}_{(1)}[\delta k_z]$ solves the differential equation $-\partial_x^2 \delta\mathcal{E}_{(1)} = -\varepsilon_z(x)/\varepsilon_x 2k_z \delta k_z$. The solution has the derivative

$$\delta\mathcal{E}'_{(1)}(x) = 2k_z \delta k_z \left[\varepsilon_x \int_0^x \varepsilon_z(\xi) d\xi \right]^{-1},$$

which enters $D[\mathbf{k}^* + \delta\mathbf{k}]$. Thus, we obtain $b_x = 0$ and

$$b_z = \left[\xi_0 - d \int_0^1 f(x) dx \right] \frac{2dk_z \varepsilon_{z,0}}{\varepsilon_x}.$$

At the critical point, the expression in the bracket must vanish, which produces Eq. (8).

A refined computation for the critical case of $d = d_0$ gives $b_{xx} = -d^2$, $b_{xz} = 0$, and $b_{zz} > 0$. Thus, the effective dispersion relation at $d/d_0 = 1$ up to second-order terms is $b_{xx} \delta k_x^2 + b_{zz} \delta k_z^2 = 0$ with $b_{xx} b_{zz} < 0$, which corresponds to a Dirac cone. Moreover, for $\varepsilon_z^{\text{eff}}/\varepsilon_x \sim 1$ it can be shown that

$$D[\mathbf{k}^* + \delta\mathbf{k}] \approx -d^2 \left[\delta k_x^2 + \frac{\varepsilon_z^{\text{eff}}}{\varepsilon_x} (k_z^* + \delta k_z)^2 - \frac{\varepsilon_z^{\text{eff}}}{\varepsilon_x} (k_z^*)^2 \right].$$

By $(k_z^*)^2/\varepsilon_x = k_0^2$, the above relation recovers the elliptic profile of Eq. (5).

In order to support this bifurcation argument with numerical evidence, we test Eq. (8) for two additional dielectric profiles which to our knowledge do not admit exact solutions in simple closed form. In the spirit of Ref. 28, we study distinctly different profiles $\varepsilon_z(x)$. Specifically, we use the symmetric double-well profile $f_{\text{dw}}(x) = 1 - 3.2x + 13.2x^2 - 20x^3 + 10x^4$ and the nonsymmetric profile $f_{\text{ns}}(x) = 1 + 0.5(e^{5x} - 1)(1 - x)$. The computational results for the dispersion relation are given in Fig. 2b-c. Furthermore, for \mathbf{k} in the neighborhood of \mathbf{k}^* and $d/d_0 = 1.1$ we notice excellent agreement of effective dispersion relation (5) with the numerically computed curve $k_z(k_x)$ (Fig. 3).

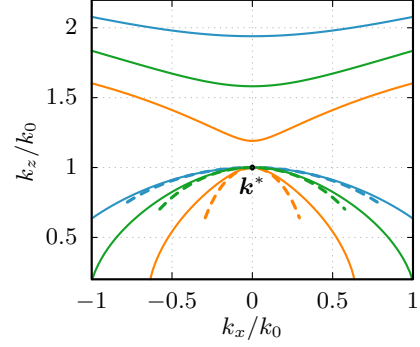


FIG. 3: Numerically computed dispersion curves (solid lines) and the effective dispersion relation Eq. 5 (dashed lines) for $d/d_0 = 1.1$ computed for the parabolic (blue), double-well $f_{\text{dw}}(x)$ (orange), and nonsymmetric profile $f_{\text{ns}}(x)$ (green). The curvatures agree at the critical point \mathbf{k}^* .

To test the results of our model against more practical configurations, we carry out direct numerical simulations for a system with a finite number of metallic sheets. We choose graphene as the material for the 2D conducting sheets, since it has been used extensively in plasmonic and optoelectronic applications^{18,23}. In the THz frequency regime, doped graphene behaves like a Drude metal because intraband transitions are dominant^{23,24}. In this frequency regime doped graphene supports plasmons²³. Hence, the conductivity of the metallic sheets is approximated by the Drude formula, $\sigma = ie^2 \mu_c / [\pi \hbar^2 (\omega + i/\tau)]$. The doping amount is $\mu_c = 0.5 \text{ eV}$ and the transport scattering time of electrons is $\tau = 0.5 \text{ ps}$ to account for optical losses^{5,6}.

In Fig. 4, we present the spatial distribution of $H_y(x, z)$ propagating through a structure of 100 graphene layers embedded periodically in a lossless dielectric host with anisotropic and spatial-dependent permittivity. The numerical computation is carried out for parabolic profile (4) with $\alpha = 20/3$, $\varepsilon_{z,0} = 2$, $\varepsilon_x = 1$, as well as the double-well profile, with $\varepsilon_{z,0} = 2$ and $\varepsilon_x = 4$. By setting the structural period to $d = d_0$, we observe the expected signature of ENZ behavior, namely, wave propagation with no phase delay through the periodic structure^{1,4,5}.

V. DISCUSSION AND CONCLUSION

In this section, we conclude our analysis by discussing implications of our approach, summarizing our results and mentioning open related problems. Of particular interest is a generalization of our result for the effective dielectric permittivity of the layered plasmonic structure. The notion of an effective permittivity $\varepsilon_z^{\text{eff}}$ that arises in Eqs. (5) and (8) bears a striking similarity to homogenization results for Maxwell's equations²⁹. In fact, it can be shown that Eq. (8) can also be derived by ap-

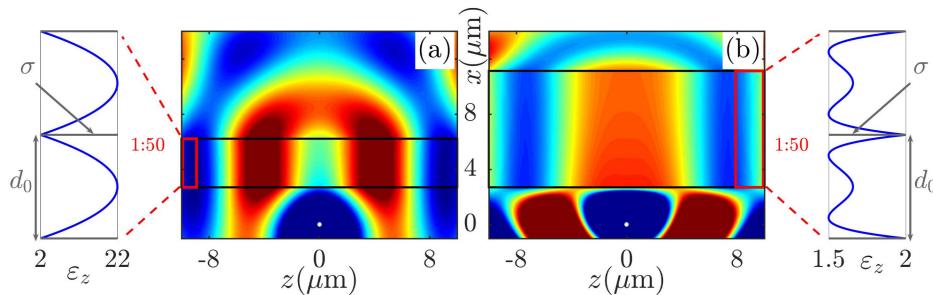


FIG. 4: Spatial distribution of H_y in an anisotropic dielectric host with 100 layers of doped graphene with structural period $d = \text{Re}(d_0)$ (black rectangle). A magnetic dipole source is located below the multilayer structures (white dots) emitting at $f = 25$ THz. The permittivity profile $\varepsilon_z(x)$ in (a) is a parabolic, and in (b) a double-well (insets). In the multilayer, waves propagate without dispersion and with no phase delay.

plying an asymptotic analysis procedure to the full system of time-harmonic Maxwell's equations. For a general tensor-valued permittivity $\underline{\varepsilon}(x/d)$ and sheet conductivity $\underline{\sigma}(x/d)$, the effective permittivity of the metamaterial takes the form

$$\underline{\varepsilon}^{\text{eff}} = \langle \underline{\varepsilon} \chi \rangle_{\text{host}} + \frac{i}{\omega} \langle \underline{\sigma} \chi \rangle_{\text{sheet}}.$$

Here, $\langle \cdot \rangle_R$ denotes the arithmetic average over region R and χ is a weight function that solves a closed boundary value problem in the individual layer³⁰. In the special case of $\underline{\varepsilon} = \text{diag}(\varepsilon_x, \varepsilon_z, \varepsilon_z)$, the weight function reduces to the unit tensor, $\chi = I$. Understanding the ENZ behavior on the basis of this more general effective permittivity is the subject of work in progress.

Our work points to several open questions. For example, we analyzed wave propagation through a plasmonic structure primarily *in absence of a current-carrying source*. A related problem is to *analytically* investigate how the dispersion band and ENZ condition derived here may affect the modes excited by dipole sources located in the proximity of a finite layered structure. This more demanding problem will be the subject of future work.

In conclusion, we have shown that dispersive Dirac cones are universal for a wide class of plasmonic multilayer systems consisting of 2D metals with isotropic, constant conductivity. We also derived a general, exact condition on the structural period d to obtain a corresponding dispersion relation with ENZ behavior. The universality of our approach is key for the investigation of wave coupling effects in discrete periodic systems and the design of effective ENZ media. Our results pave the way to a systematic study of homogenization and effective parameters in the context of more general multilayer plasmonic systems.

ACKNOWLEDGMENTS

We acknowledge support by ARO MURI Award No. W911NF-14-0247 (MMai, MMat, EK, ML, DM); EFRI 2-DARE NSF Grant No. 1542807 (MMat); and NSF DMS-1412769 (DM). We used computational resources on the Odyssey cluster of the FAS Research Computing Group at Harvard University.

Appendix A: Exact solution for parabolic dielectric profile

In this appendix, we outline the derivation of the exact dispersion relation for parabolic dielectric profile (4). As a first step, we characterize the general solution of the differential equation

$$-\partial_x^2 \mathcal{E}(x) + \kappa(k_z) \varepsilon_z(x) \mathcal{E}(x) = 0, \quad \kappa(k_z) = \frac{k_z^2 - k_0^2 \varepsilon_x}{\varepsilon_x},$$

where the free space permittivity is set $\varepsilon_0 = 1$ and $k_0 = \omega \sqrt{\mu}$. In order to derive the solution of the above differential equation, we apply a change of coordinate from x to χ , viz.,

$$x \rightarrow \chi = \rho \left(\frac{x}{d} - \frac{1}{2} \right),$$

using a complex-valued scaling parameter, ρ , to be determined below. By identifying $\tilde{\mathcal{E}}(\chi) = \mathcal{E}(x)$ the differential equation now reads

$$-\partial_\chi^2 \tilde{\mathcal{E}}(\chi) + \kappa(k_z) \varepsilon_{z,0} \frac{1}{\rho^2} \left(1 + \frac{6}{4} \alpha - 6\alpha \frac{1}{\rho^2} \chi^2 \right) \tilde{\mathcal{E}}(\chi) = 0.$$

We now fix ρ by the requirement that

$$-6\alpha \frac{1}{\rho^4} \kappa(k_z) \varepsilon_{z,0} = \frac{1}{4}.$$

342 Thus, if $\alpha \leq 0$, we set

$$\rho(\alpha) = \left(-24 \alpha \kappa(k_z) \varepsilon_{z,0} \right)^{1/4}. \quad (\text{A1})$$

343 We can analytically continue the above function $\rho(\alpha)$
344 to values $\alpha > 0$ by properly choosing one of the
345 four branches of the (complex) multiple-valued function
346 $w(z) = z^{1/4}$. By the definition

$$\nu = -1 - \sqrt{\kappa(k_z) \varepsilon_{z,0}} \frac{1 + (3/2)\alpha}{(-24\alpha)^{1/2}},$$

347 the transformed differential equation for $\tilde{\mathcal{E}}(\chi)$ takes the
348 canonical form

$$-\partial_\chi^2 \tilde{\mathcal{E}}(\chi) + \left(\frac{1}{2} \chi^2 - \nu - \frac{1}{2} \right) \tilde{\mathcal{E}}(\chi) = 0.$$

349 This differential equation has the general solution

$$\tilde{\mathcal{E}}(\chi) = C_1 D_\nu(\chi) + C_2 D_\nu(-\chi), \quad (\text{A2})$$

350 where $D_\nu(\chi)$ is the parabolic cylinder or Weber-Hermite
351 function, given by the formula

$$D_\nu(\chi) = 2^{\nu/2} e^{-\chi^2/4} \left[\frac{\Gamma(1/2)}{\Gamma(1/2 - \nu/2)} \Phi(-\nu/2, 1/2; \chi^2/2) \right. \\ \left. + \frac{\chi}{2^{1/2}} \frac{\Gamma(-1/2)}{\Gamma(-\nu/2)} \Phi(1/2 - \nu/2, 3/2; \chi^2/2) \right],$$

352 and C_1 and C_2 are integration constants. In the above,
353 $\Gamma(z)$ is the Gamma function and $\Phi(a, b; z)$ is the confluent
354 hypergeometric function defined by the power series

$$\Phi(a, b; z) = \sum_{n=0}^{\infty} \frac{(a)_n z^n}{(b)_n n!},$$

355 where $(a)_0 = 1$, $(a)_n = (a + n - 1)(a)_{n-1}$ for $n \geq 1$.

356 To derive the corresponding exact dispersion relation,
357 we need to identify the fundamental solutions $\tilde{\mathcal{E}}_{(j)}(x)$
358 ($j = 1, 2$) and then substitute general solution (A2)
359 written in terms of these $\tilde{\mathcal{E}}_{(j)}(x)$ into determinant con-
360 dition (3). The resulting condition reads

$$D[\mathbf{k}] = \det \left(e^{ik_x d} \begin{bmatrix} 1 & 0 \\ -i(\sigma/\omega)\kappa(k_z) & 1 \end{bmatrix} \right. \\ \left. - \begin{bmatrix} \tilde{\mathcal{E}}_{(1)}(\rho/2) & \tilde{\mathcal{E}}_{(2)}(\rho/2) \\ \tilde{\mathcal{E}}'_{(1)}(\rho/2) & \tilde{\mathcal{E}}'_{(2)}(\rho/2) \end{bmatrix} \right) = 0.$$

361 After some algebra, the exact dispersion relation reads

$$\cos(k_x d) + \frac{\Gamma(-\nu)}{\sqrt{2\pi}} \left\{ D_\nu(-\rho/2) D'_\nu(-\rho/2) \right. \\ \left. + D_\nu(\rho/2) D'_\nu(\rho/2) \right. \\ \left. - \frac{\kappa(k_z) \varepsilon_{z,0} \xi_0 d}{2\rho} [D_\nu(\rho/2)^2 - D_\nu(-\rho/2)^2] \right\} = 0. \quad (\text{A3})$$

362 Here, $\xi_0 = -i\sigma/(\omega\varepsilon_{z,0})$ is the plasmonic thickness. Note
363 that, by our construction, ρ and ν are k_z dependent,
364 viz., $\rho = \rho(k_z)$ and $\nu = \nu(k_z)$. Thus, Eq. (A3) still
365 expresses an implicit relationship between k_x and k_z . To
366 further simplify Eq. (A3), we expand $D_\nu(\rho/2)$ to fourth
367 order in z . For sufficiently small structural period, d , i.e.,
368 $|\kappa(k_z)d| \ll 1$, and after some algebraic manipulations the
369 exact dispersion relation simplifies to

$$\cos(k_x d) \approx 1 - \frac{\kappa(k_z) \varepsilon_{z,0} \xi_0 d}{2} - (2\nu + 1)(-3/2)\alpha^{1/2} \\ \times \left(\sqrt{\kappa(k_z) \varepsilon_{z,0}} d \right) - \frac{1}{4} \alpha \kappa(k_z) \varepsilon_{z,0} d^2.$$

370 Furthermore, in the vicinity of Brillouin zone center, i.e.,
371 if $|k_x d| \ll 1$, we apply the Taylor expansion $\cos(k_x d) \approx$
372 $1 - (1/2) k_x^2 d^2$ and use the definitions of ν and $\kappa(k_z)$ to
373 obtain the *effective* dispersion relation

$$\frac{k_x^2}{\varepsilon_z^{\text{eff}}} + \frac{k_z^2}{\varepsilon_x} = k_0^2, \quad \frac{\varepsilon_z^{\text{eff}}}{\varepsilon_{z,0}} = 1 + \alpha - \frac{\xi_0}{d},$$

374 which is identical to Eq. (5).

375 Appendix B: Numerical scheme for computation of 376 dispersion bands

377 In this appendix, we present more details on the nu-
378 merical procedure to compute dispersion bands for arbi-
379 trary dielectric profiles $\varepsilon_z(x)$. For given problem param-
380 eters σ , ω , and profile $\varepsilon_z(x)$, and fixed real k_x , consider
381 the task of finding a complex-valued solution k_z of (3).

382 We formulate a Newton method in order to solve the
383 implicit dispersion relation $D[\mathbf{k}] = 0$ numerically. For
384 this purpose, we first need to characterize the variation
385 $\delta\mathcal{E}_{(i)}$ of solutions $\mathcal{E}_{(i)}$ of Eq. (1) with respect to k_z . We
386 make the observation that $\delta\mathcal{E}_{(i)}$ is the unique solution of
387 the differential equation

$$-\partial_x^2 \delta\mathcal{E}_{(i)} + \kappa(k_z) \varepsilon_z(x) \delta\mathcal{E}_{(i)} + \kappa'(k_z) \varepsilon_z(x) \mathcal{E}_{(i)} = 0,$$

388 where

$$\kappa'(k_z) = \frac{2k_z}{\varepsilon_x},$$

$$\delta\mathcal{E}_{(i)}(0) = 0, \quad \delta\mathcal{E}'_{(i)}(0) = 0.$$

389 With this prerequisite at hand, the variation of $D[\mathbf{k}]$ with
390 respect to k_z can be expressed as follows:

$$\delta D[\mathbf{k}] = -e^{ik_x d} \left\{ \delta\mathcal{E}_{(1)}(d) (1 - \mathcal{E}'_{(2)}(d)) \right. \\ \left. + (1 - \mathcal{E}_{(1)}(d)) \delta\mathcal{E}'_{(2)}(d) \right. \\ \left. + (i(\sigma/\omega)\kappa'(k_z) + \delta\mathcal{E}'_{(1)}(d)) \mathcal{E}_{(2)}(d) \right. \\ \left. + (i(\sigma/\omega)\kappa(k_z) + \mathcal{E}'_{(1)}(d)) \delta\mathcal{E}_{(2)}(d) \right\}. \quad (\text{B1})$$

391 Next, we outline the steps of the Newton scheme. Let
392 k_x be fixed. Suppose that starting from an initial guess

393 $k_z^{(0)}$ we have computed an approximate solution $k_z^{(n)}$ of 399
 394 Eq. (3). We then compute a new approximation $k_z^{(n+1)}$
 according to the following sequence of steps:

395

396 • Solve the first order systems ($i = 1, 2$)

$$\begin{cases} -\partial_x(\mathcal{E}'_{(i)}) + \kappa(k_z)\varepsilon_z(x)\mathcal{E}_{(i)} = 0, \\ -\partial_x(\mathcal{E}_{(i)}) = \mathcal{E}'_{(i)}, \end{cases}$$

397 with initial conditions $\mathcal{E}_{(1)}(0) = 1$, $\mathcal{E}'_{(1)}(0) = 0$,
 398 $\mathcal{E}_{(2)}(0) = 0$, $\mathcal{E}'_{(2)}(0) = 1$.

• Solve the systems ($i = 1, 2$)

$$\begin{cases} -\partial_x(\delta\mathcal{E}'_{(i)}) + \kappa(k_z)\varepsilon_z(x)\delta\mathcal{E}_{(i)} + \kappa'(k_z)\varepsilon_z(x)\mathcal{E}_{(i)} = 0, \\ -\partial_x(\delta\mathcal{E}_{(i)}) = \delta\mathcal{E}'_{(i)}, \\ \partial\mathcal{E}_{(i)}(0) = 0, \quad \partial\mathcal{E}'_{(i)}(0) = 0. \end{cases}$$

400 • Compute $D[k_x, k_z^{(n)}]$ and $\delta D[k_x, k_z^{(n)}]$ given by
 401 Eqs. (3) and (B1).

402 • Update:

$$k_z^{(n+1)} = k_z^{(n)} - \frac{D[k_x, k_z^{(n)}]}{\delta D[k_x, k_z^{(n)}]}.$$

403 * msmaier@umn.edu; <http://www.math.umn.edu/~msmaier>
 404 † mariosmat@g.harvard.edu; http://scholar.harvard.edu/marios_matthaiakis
 405
 406 ¹ M. Silveirinha and N. Engheta, Phys. Rev. Lett. **97**, 157403
 407 (2006).
 408 ² X. Huang, Y. Lai, Z. H. Hang, H. Zheng, and C. T. Chan,
 409 Nat. Mater. **10**, 582 (2011).
 410 ³ P. Moitra, Y. Yang, Z. Anderson, I. I. Kravchenko, D. P.
 411 Briggs, and J. Valentine, Nat. Photon **7**, 791 (2013).
 412 ⁴ Y. Li, S. Kita, P. Munoz, O. Reshef, D. I. Vulis, M. Yin,
 413 M. Loncar, and E. Mazur, Nat. Photon **9**, 738 (2015).
 414 ⁵ M. Mattheakis, C. A. Valagiannopoulos, and E. Kaxiras,
 415 Physical Review B **94**, 201404(R) (2016).
 416 ⁶ B. Wang, X. Zhang, F. J. Garca-Vidal, X. Yuan, and
 417 J. Teng, Physical Review Letters **109**, 073901 (2012).
 418 ⁷ D. Wintz, P. Genevet, A. Ambrosio, A. Wolf, and F. Ca-
 419 passio, Nano Letters **15**, 3585 (2015), pMID: 25915541.
 420 ⁸ S. Dai, Q. Ma, M. K. Liu, T. Andersen, Z. Fei, M. D.
 421 Goldflam, M. Wagner, K. Watanabe, T. Taniguchi,
 422 M. Thiemens, F. Keilmann, G. C. A. M. Janssen, S.-E.
 423 Zhu, P. Jarillo-Herrero, M. M. Fogler, and D. N. Basov,
 424 Nat. Nano **10**, 682 (2015).
 425 ⁹ A. Nemilentsau, T. Low, and G. Hanson, Phys. Rev. Lett.
 426 **116**, 066804 (2016).
 427 ¹⁰ D. R. Smith, Science **345**, 384 (2014).
 428 ¹¹ A. Alù and N. Engheta, Phys. Rev. E **72**, 016623 (2005).
 429 ¹² T. Zentgraf, Y. Liu, M. H. Mikkelsen, J. Valentine, and
 430 X. Zhang, Nat. Nano **6**, 151 (2011).
 431 ¹³ J. Cheng, W. L. Wang, H. Mosallaei, and E. Kaxiras,
 432 Nano Letters **14**, 50 (2014).
 433 ¹⁴ A. A. High, R. C. Devlin, A. Dibos, M. Polking, D. S.
 434 Wild, J. Perczel, N. P. de Leon, M. D. Lukin, and H. Park,
 435 Nature **522**, 192 (2015).
 436 ¹⁵ S. V. Zhukovsky, A. Andryeuskii, J. E. Sipe, and A. V.

437 Lavrinenko, Phys. Rev. B **90**, 155429 (2014).
 438 ¹⁶ H. Deng, F. Ye, B. A. Malomed, X. Chen, and N. C.
 439 Panoiu, Phys. Rev. B **91**, 201402 (2015).
 440 ¹⁷ P. Mirò, M. Audiffred, and T. Heine, Chem. Soc. Rev. **43**,
 441 6537 (2014).
 442 ¹⁸ F. Xia, H. Wang, D. Xiao, M. Dubey, and A. Ramasub-
 443 ramaniam, Nat. Photon **8**, 899 (2014).
 444 ¹⁹ I. V. Iorsh, I. S. Mukhin, I. V. Shadrivov, P. A. Belov, and
 445 Y. S. Kivshar, Phys. Rev. B **87**, 075416 (2013).
 446 ²⁰ B. Wang, X. Zhang, K. P. Loh, and J. Teng, Journal of
 447 Applied Physics **115**, 213102 (2014).
 448 ²¹ M. Jablan, H. Buljan, and M. Soljačić, Phys. Rev. B **80**,
 449 245435 (2009).
 450 ²² T. Low, A. Chaves, J. D. Caldwell, A. Kumar, N. X. Fang,
 451 P. Avouris, T. F. Heinz, F. Guinea, L. Martin-Moreno,
 452 and F. Koppens, Nat. Mater **16**, 182 (2017).
 453 ²³ A. N. Grigorenko, M. Polini, and K. S. Novoselov, Nat.
 454 Photon **6**, 749 (2012).
 455 ²⁴ Z. Fei, A. S. Rodin, G. O. Andreev, W. Bao, A. S.
 456 McLeod, M. Wagner, L. M. Zhang, Z. Zhao, M. Thiemens,
 457 G. Dominguez, M. M. Fogler, A. H. C. A. H. Neto, C. N.
 458 Lau, F. Keilmann, and D. N. Basov, Nature **487**, 85
 459 (2012).
 460 ²⁵ S. N. Shirodkar, M. Mattheakis, P. Cazeaux, P. Narang,
 461 M. Soljačić, and E. Kaxiras, Arxiv **1703.01558** (2017).
 462 ²⁶ M. Born and E. Wolf, Optics and Laser Technology **7**, 190
 463 (1975).
 464 ²⁷ M. Mattheakis, G. P. Tsironis, and V. I. Kovanis, Journal
 465 of Optics **14**, 114006 (2012).
 466 ²⁸ A. Roger, D. Maystre, and M. Cadilhac, J. Optics (Paris)
 467 **9**, 83 (1978).
 468 ²⁹ N. Wellander and G. Kristensson, SIAM Journal of Ap-
 469 plied Mathematics **64**, 170 (2003).
 470 ³⁰ M. Maier, D. Margetis, M. Luskun, M. Mattheakis, and
 471 E. Kaxiras, Paper in preparation. (2017).